



# Discovery of Genetic Biomarkers for Alzheimer's Disease Using Adaptive Convolutional Neural Networks Ensemble and Genome-Wide Association Studies

An Zeng<sup>1</sup> · Huabin Rong<sup>1</sup> · Dan Pan<sup>2</sup> · Longfei Jia<sup>1</sup> · Yiqun Zhang<sup>1</sup> · Fengyi Zhao<sup>1</sup> · Shaoliang Peng<sup>3</sup> · for the Alzheimer's Disease Neuroimaging Initiative (ADNI)

Received: 21 February 2021 / Revised: 1 July 2021 / Accepted: 1 August 2021  
© International Association of Scientists in the Interdisciplinary Areas 2021

## Abstract

**Objective** To identify candidate neuroimaging and genetic biomarkers for Alzheimer's disease (AD) and other brain disorders, especially for little-investigated brain diseases, we advocate a data-driven approach which incorporates an adaptive classifier ensemble model acquired by integrating Convolutional Neural Network (CNN) and Ensemble Learning (EL) with Genetic Algorithm (GA), i.e., the CNN-EL-GA method, into Genome-Wide Association Studies (GWAS).

**Methods** Above all, a large number of CNN models as base classifiers were trained using coronal, sagittal, or transverse magnetic resonance imaging slices, respectively, and the CNN models with strong discriminability were then selected to build a single classifier ensemble with the GA for classifying AD, with the help of the CNN-EL-GA method. While the acquired classifier ensemble exhibited the highest generalization capability, the points of intersection were determined with the most discriminative coronal, sagittal, and transverse slices. Finally, we conducted GWAS on the genotype data and the phenotypes, i.e., the gray matter volumes of the top ten most discriminative brain regions, which contained the ten most points of intersection.

**Results** Six genes of PCDH11X/Y, TPTE2, LOC107985902, MUC16 and LINC01621 as well as Single-Nucleotide Polymorphisms, e.g., rs36088804, rs34640393, rs2451078, rs10496214, rs17016520, rs2591597, rs9352767 and rs5941380, were identified.

**Conclusion** This approach overcomes the limitations associated with the impact of subjective factors and dependence on prior knowledge while adaptively achieving more robust and effective candidate biomarkers in a data-driven way.

**Significance** The approach is promising to facilitate discovering effective candidate genetic biomarkers for brain disorders, as well as to help improve the effectiveness of identified candidate neuroimaging biomarkers for brain diseases.

**Keywords** Alzheimer's disease · Neuroimaging · Deep learning · Ensemble learning · Genetic algorithm · Single-nucleotide polymorphism · Genome-wide association studies

---

Alzheimer's Disease Neuroimaging Initiative-Data used in preparation of this article were obtained from the Alzheimer's Disease Neuroimaging Initiative (ADNI) database (adni.loni.usc.edu). As such, the investigators within the ADNI contributed to the design and implementation of ADNI and/or provided data but did not participate in analysis or writing of this report. A complete listing of ADNI investigators can be found at: [http://adni.loni.usc.edu/wpcontent/uploads/how\\_to\\_apply/ADNI\\_Acknowledgement\\_List.pdf](http://adni.loni.usc.edu/wpcontent/uploads/how_to_apply/ADNI_Acknowledgement_List.pdf).

✉ Dan Pan  
pandan@gpnu.edu.cn

✉ Shaoliang Peng  
slpeng@hnu.edu.cn; pengshaoliang@nudt.edu.cn

Extended author information available on the last page of the article

## 1 Introduction

Alzheimer's disease (AD) involves progressive neurodegeneration, causing cognitive decline, and the loss of memory and other brain functions. The patients will suffer from amnesia, low mobility, language disability, and other adverse manifestations [1, 2] with the deterioration of the disease. Mild Cognitive Impairment (MCI) is a transition stage between the natural cognitive deterioration of normal aging and the more severe deterioration of AD. Existing studies [3] have shown that patients with MCI are further categorized into those who will convert to AD (MCIc) and those who will not convert to AD (MCInc) in a short period of

time, compared with age-matched Healthy Cognition (HC). Therefore, how to accurately determine the disease stage of a patient has become the research focus in screening AD.

Structural Magnetic Resonance Imaging (sMRI) can be noninvasively utilized to examine anatomical and pathological changes in the brain. Especially, the atrophy of hippocampus and entorhinal cortex captured by it can reflect the disease stage to a certain extent and help predict the progression of MCI to AD [4]. Thus, MRI is widely adopted in the study of AD diagnosis [5–12]. The results obtained by traditional feature extraction methods for capturing MRI structural changes largely depended on the manual skills [13], which required a large amount of prior knowledge. In contrast, as a data-driven machine-learning method, deep learning enables the acquired model to be more flexible, universal, and objective since training a deep-learning model is an automated learning process with eliminating the need of manually extracting features.

In recent years, Convolution Neural Networks (CNNs) [14] have shown their superiority in various fields. Excellent image feature extraction capabilities have also made CNNs very popular in the field of medical image analysis [15, 16]. A deep three-dimensional (3D) CNN method was used to learn the discriminative features of MRI to predict AD [17]. Since a large amount of training data are required during training CNN, the CNN model pre-trained on the ImageNet dataset was employed to extract the features of MRI using transfer learning [18]; a content-based image retrieval system using 3D capsule network, 3D convolutional neural network and pre-trained 3D autoencoder technology were advocated for early detection of AD [19].

At the same time, Ensemble Learning (EL) has exhibited the benefits of performance and robustness by integrating multiple learning systems. More and more studies have exhibited that deep learning combined with EL techniques has given promising results by modeling MRI data with high accuracy for early diagnosis of AD [20]. An ensemble of 3D densely connected convolutional networks (3DDenseNets) has been proposed for classifying AD and MCI using T1-weighted MRIs [21]. Plus, in [22], Pan et al. decomposed a three-dimensional MRI into two-dimensional slices along the coronal, sagittal and transverse planes, and trained a based classifier (i.e., a CNN model here) corresponding to a two-dimensional slice. The five base classifiers with the best generalization performance on the validation dataset were chosen among the coronal, sagittal and transverse slice-based base classifiers, respectively. Finally, a classifier ensemble based on three-axis slices was built with the three

classifier ensembles based on coronal, sagittal and transverse slices, respectively, following a simple majority voting scheme. Thus, based on these, the discriminative brain regions were discerned. This method effectively improved the diagnosis of AD, but the number of the chosen best base classifiers, i.e., 15, was manually determined. To solve this problem, Genetic Algorithm (GA) was introduced to adaptively select the best base classifiers for building the final classifier ensemble with the highest generalization capability in a data-driven manner in this study. In addition, although the above methods captured the salient features of MRI to some degree with CNNs, these features were only used to detect diseases or determine relevant brain regions, but failed to perform correlation analysis between related brain regions and genes to help discover the candidate genetic biomarkers.

Image genetics is an active research field emerging with the accumulation of high-throughput omics data and multimodal imaging data. The main purpose is to acquire effective information from multimodal imaging data and omics data, such as Single-Nucleotide Polymorphism (SNP) and proteomics data [23]. Some researchers have performed Genome-Wide Association Studies (GWAS) between AD locus and MRI biomarkers [24]. Tan et al. conducted GWAS experiments on related loci with late-onset AD in Han population in northern China [25]. Studies have shown that AD is affected by genetic factors, and the discovery of genetic biomarkers for AD is of important clinical significance.

In this study, above all, we proposed an adaptive classifier ensemble model by combining CNN and EL with Genetic Algorithm (GA), i.e., the CNN-EL-GA approach, to automatically extract features that can be employed to distinguish subjects with clinical diagnosis of AD or MCI from HC, and to distinguish the subjects with MCIc from those with MCInc, using brain MRI data. For each of three binary classification tasks in this study, the five-fold cross-validation procedure was rigorously observed to avoid the potential data leakage. First, a 3D MRI image was pre-processed and the base classifiers were trained in the same way as that in [22]. To prevent introducing subjective factors in the process of selecting the trained base classifiers to build the classifier ensemble, we adopted genetic algorithm (GA) to optimize the selection process in a data-driven manner. In this way, the optimal combination of base classifiers was ultimately determined to build a refined classifier ensemble with the help of GA. Subsequently, the intersection points and the most discriminative brain regions were decided in the same way as that described in [22] while the acquired

ensemble model exhibited the highest generalization capability. Finally, gray matter volumes of the top ten most discriminative brain regions, as phenotypes, together with the genotype were employed to conduct GWAS experiments to discover the candidate genetic biomarkers for AD.

## 2 Materials and Methods

### 2.1 Participants and datasets

Data used in the study were obtained from the Alzheimer's Disease Neuroimaging Initiative (ADNI) database. The ADNI was launched in 2003 as a public-private partnership, led by Principal Investigator, Michael W. Weiner, MD. The primary goal of ADNI has been to test whether serial MRI, positron emission tomography (PET), other biological markers, and clinical and neuropsychological assessment can be combined to measure the progression of MCI and early AD.

Here, among the 509 subjects involved in [26], the 458 subjects (AD = 122, MCIc = 70, MCIinc = 118 and HC = 148) with MRI and SNP data available for download were selected. Their MRI and SNP data were retrieved from the ADNI database to train the base classifiers and to examine the performance of the final classifier ensemble. Since there was a need for additional MRI data to acquire the optimal combination of base classifiers, we downloaded the MRI data of additional 278 subjects (AD = 100, MCIc = 39, MCIinc = 39, and HC = 100) in the ADNI database to act as a validation dataset. There was no overlapping between the 458 subjects and the 278 subjects. Tables 1 and 2 show the subjects' gender, age, weight, Clinical Dementia Rating (CDR), Geriatric Depression Scale (GDS) and Mini-Mental State Examination (MMSE) scale.

**Table 1** Information on the subjects in the training and testing datasets

Participant group	Male/female	Age/year	Weight/kg	MMSE	CDR	GDS
AD ( <i>N</i> = 122)	60/62	76.00 ± 7.10	70.92 ± 13.33	23.21 ± 2.04	0.76 ± 0.25	1.59 ± 1.30
MCIc ( <i>N</i> = 70)	41/29	74.93 ± 7.29	72.45 ± 14.42	26.51 ± 1.91	0.50 ± 0.00	1.44 ± 1.16
MCIinc ( <i>N</i> = 118)	75/43	74.35 ± 6.99	76.21 ± 13.38	27.16 ± 1.72	0.50 ± 0.00	1.56 ± 1.42
HC ( <i>N</i> = 148)	73/75	76.00 ± 5.26	74.42 ± 13.35	29.18 ± 0.96	0.00 ± 0.00	0.81 ± 1.08

**Table 2** Information on the subjects in the validation dataset

Participant group	Male/Female	Age/year	Weight/kg	MMSE	CDR	GDS
AD ( <i>N</i> = 100)	60/40	74.24 ± 7.82	76.04 ± 15.83	23.84 ± 2.08	0.82 ± 0.24	1.81 ± 1.56
MCIc ( <i>N</i> = 39)	23/16	74.15 ± 7.10	73.59 ± 14.14	27.05 ± 1.59	0.50 ± 0.00	1.92 ± 1.35
MCIinc ( <i>N</i> = 39)	29/10	76.02 ± 7.00	78.35 ± 12.99	27.56 ± 1.83	0.50 ± 0.00	1.79 ± 1.45
HC ( <i>N</i> = 100)	45/55	73.36 ± 5.70	76.16 ± 15.66	28.92 ± 1.25	0.00 ± 0.00	0.83 ± 1.34

### 2.2 Methods

The pipeline of the proposed approach incorporating the CNN-EL-GA method into GWAS for discovering candidate genetic biomarkers for AD is shown in Fig. 1. It is divided into four main components: (1) preprocessing image and gene data; (2) training base classifiers; (3) optimizing the combination of base classifiers and ensembling; (4) discovering the candidate genetic biomarkers with GWAS, i.e., identifying the brain regions with stronger discriminability and calculating their gray matter volumes to discover statistically significant SNPs associated with the phenotype for AD with GWAS.

#### 2.2.1 Image Preprocessing

The CAT12 toolkit (<https://www.neuro.uni-jena.de/cat/>) with default value setting was employed to preprocess the T1-weighted MRI data in nii format retrieved from ADNI database. The involved steps included non-brain tissue removal, registration to MNI space, image smooth with SPM12 (<https://www.fil.ion.ucl.ac.uk/spm/software/spm12/>), normalization, slicing and resizing. The dimension of each smoothed image was 121 × 145 × 121. After slicing, resizing and selecting, a total of 123 slices (of 145 × 145) from a subject's 3D MRI image, i.e., 40 sagittal slices, 50 coronal slices, and 33 transverse slices, were obtained. The image preprocessing steps are shown in Fig. 2. For further details, please refer to [22].

#### 2.2.2 Gene Data Preprocessing

The ADNI database provides not only medical imaging data, such as MRI and PET, but also a large amount of genotype data, e.g., 620,901 SNPs. The genotypic data of the 458 subjects described in Table 1 were downloaded and saved in three files with suffixes of .BIM, .FAM and .BED,

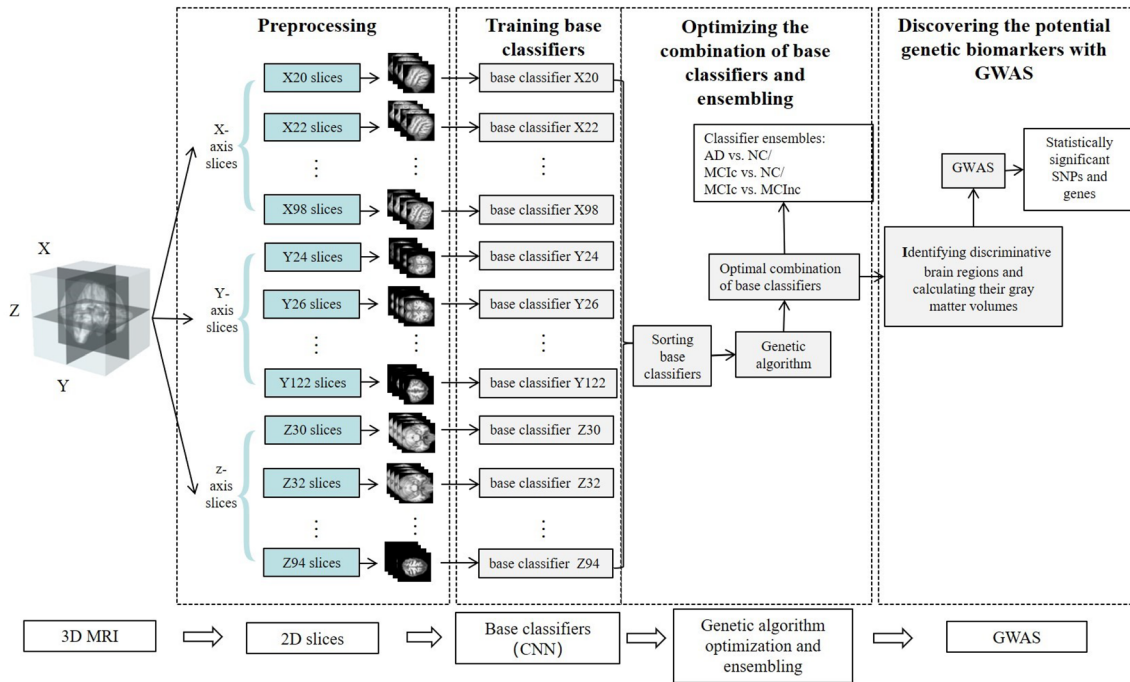
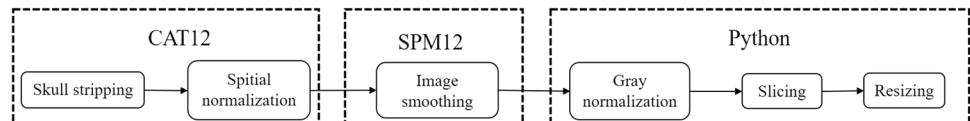


**Fig. 1** The pipeline of the proposed approach incorporating the CNN-EL-GA method into GWAS for discovering candidate genetic biomarkers for AD

**Fig. 2** Image preprocessing steps



i.e., the standard PLINK [27] files. The phenotypic data in the GWAS experiments were the morphological parameters (gray matter volume values, here) of brain regions with strong discriminability in classifying AD, which were calculated by FreeSurfer-v6.0.0 [28] ([https://surfer.nmr.mgh.harvard.edu/pub/dist/freesurfer/6.0.0/freesurfer-Linuxcentos6\\_x86-64-stable-pub-v6.0.0.tar.gz](https://surfer.nmr.mgh.harvard.edu/pub/dist/freesurfer/6.0.0/freesurfer-Linuxcentos6_x86-64-stable-pub-v6.0.0.tar.gz)) after the "Brainetome Atlas [29]" was imported into it.

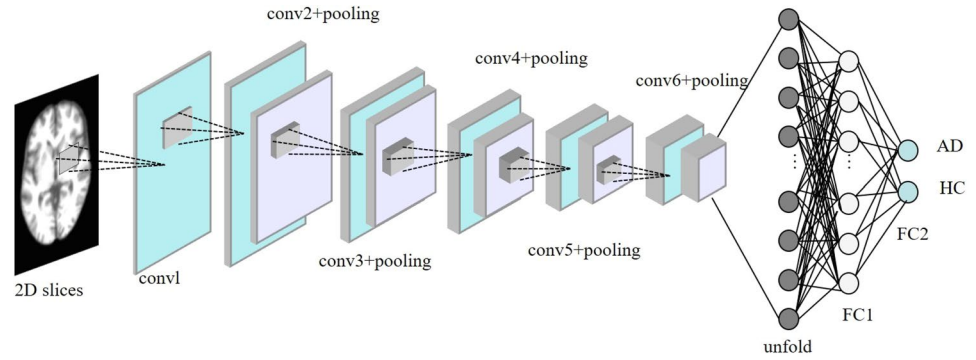
To eliminate the negative effects of data issues (e.g., low quality of DNA samples, sample contamination and population stratification) on GWAS, appropriate quality control procedures were applied on genotype data in this study. The PLINK v1.90b5.2 64 package (<https://www.cog-genomics.org/plink/1.9>) was employed to finish the following steps, i.e., screening subjects based on the heterozygosity rate, the

locus deletion rate and individual independence, respectively; filtering locus based on the deletion rate of locus, the Hardy–Weinberg equilibrium law and the linkage disequilibrium, respectively; correcting the population stratification with the eigenvector matrix calculate by PCA (principal component analysis). Subsequently, the obtained genotype data were employed to conduct GWAS.

### 2.2.3 Base Classifiers

The base classifier was essentially based on a 2D-CNN model with 8 layers [30], which is shown in Fig. 3. Each a base classifier was composed of six convolutional layers (conv) and two fully connected layers (FCs). The corresponding hyper-parameters are shown in [22]. The pooling

**Fig. 3** The architecture of base classifiers utilized in the CNN-EL-GA approach



operation was not involved in the first convolutional layer but involved in the last five convolutional layers. And normalized exponential function, i.e., softmax function, was employed to yield the outputs of the two neurons in the last full connected layer between 0 and 1, which could be understood as the probability estimation of the predicted class labels, e.g., AD and HC.

The features of 2D slices were extracted by the convolutional layers in the base classifiers. In each convolutional layer, a set of kernels (filters) were utilized to extract specific features from the outputs of the previous layer.

The same parameter setting as shown in [22] was applied to each base classifier.

#### 2.2.4 GA-Based Classifier Ensemble

In this study, the predictions of multiple base classifiers were fused together to jointly determine the label of an unseen instance through ensemble learning. The process of optimizing the combination of base classifiers was further refined using GA and ensemble method, as shown in Algorithm 1.

In Algorithm 1, after 123 base classifiers were trained with the training dataset, the validation dataset was utilized to verify the generalization abilities of the trained base classifiers. Subsequently, based on the performance of the trained base classifiers, those with stronger generalization ability were selected to build the final classifier ensemble

with the help of GA. To speed up GA convergence, 123 base classifiers were first sorted in descending order according to their classification accuracy on the validation dataset. Then, randomly initialized a population of chromosomes. A chromosome was a 0/1 string with the length of the number of the base classifiers, i.e., A gene  $i$  in a chromosome represented a base classifier. The base classifier corresponding to the gene  $i$  appearing to be "1" was set as the selected, i.e.,  $chrom(i) = 1$ , while that corresponding to the gene  $j$  appearing to be "0" was set as the non-selected, i.e.,  $chrom(j) = 0$ . At the same time, to enable the trained base classifiers with stronger generalization ability to be more likely selected to build the final classifier ensemble, we let the mutation probabilities of a gene varied from the location of the gene in the chromosome since the base classifiers corresponding to the genes had been sorted in descending order in terms of their classification performance on the validation dataset. The formulas to calculate the mutation probability are as follows:

$$mp(pos) = \frac{pos \times p}{L}, 1 \leq pos \leq L \text{ and } chrom(pos) = 1 \quad (1)$$

$$mp(pos) = \frac{L - pos}{L} \times p, 1 \leq pos \leq L \text{ and } chrom(pos) = 0 \quad (2)$$

**Algorithm1** CNN-EL-GA

**Input:** Base classifiers  $F = \{f_1, f_2, \dots, f_L\}$ , validation dataset  $S$ , validation dataset label  $Y$ , chromosome population size  $m$ , crossover probability  $C_p$ , mutation probability  $p$ , maximum iterations  $max\_iter$ , the total number of base classifiers  $L$

**Output:** Best chromosome  $Bestchrom$

```

1:  $F \leftarrow sorted(F, S)$  \ \ Sorted in descending order according to their classification accuracy on the validation dataset
2: Randomly initialize a population of chromosomes  $P(0) \in R^{m \times L}$ 
3:  $Maxfitness \leftarrow 0$ ,  $iter \leftarrow 0$ ,  $Bestchrom \leftarrow \mathbf{0}$ 
4: while  $iter \leq max\_iter$  do
5:   for  $i \leftarrow 1$  to  $m$  do
6:      $fitness_i \leftarrow Ensemble(F \leftarrow F, T \leftarrow S, Y \leftarrow Y, chrom \leftarrow P(iter)_i)$ 
7:     if  $fitness_i > Maxfitness$  then
8:        $Maxfitness \leftarrow fitness_i$ 
9:        $Bestchrom \leftarrow P(iter)_i$ 
10:    end if
11:   end for
12:    $P(iter + 1) \leftarrow selection(P(iter), fitness)$ 
13:   for  $i \leftarrow 1$  to  $m$  do
14:     if  $rand() < C_p$  then
15:        $P(iter + 1)_i \leftarrow crossover(P(iter + 1)_i)$ 
16:     end if
17:   end for
18:   for  $i \leftarrow 1$  to  $m$  do
19:      $pos \leftarrow rand(L)$  \ \ Randomly generate a mutation position
20:     if  $P(iter + 1)_{i, pos} == 1$  then
21:        $mp \leftarrow \frac{pos \times p}{L}$ 
22:     else
23:        $mp \leftarrow \frac{L - pos}{L} \times p$ 
24:     end if
25:     if  $rand() < mp$  then
26:        $P(iter + 1)_{i, pos} \leftarrow P(iter + 1)_{i, pos} XOR 1$ 
27:     end if
28:   end for
29: end while
30: return  $Bestchrom$ 

```

**Algorithm2** Ensemble

**Input:** Base classifiers  $F = \{f_1, f_2, \dots, f_L\}$ , dataset  $T$ , label  $Y$ , chromosome  $chrom$ , the total number of base classifiers  $L$ .

**Output:** Classification performance  $performance$

```

1:  $Predict \leftarrow \mathbf{0}$ 
2: for  $i \leftarrow 1$  to  $L$  do
3:   if  $chrom_i == 1$  then
4:      $res \leftarrow f_i(T)$  \ \ Classification result for a selected base classifier
5:      $Predict \leftarrow Predict + res$  \ \ Ensembling
6:   end if
7: end for
8:  $Predict \leftarrow argmax(Predict, axis \leftarrow 1)$  \ \ Vote
9: calculate  $performance$  by  $Predict$  and  $Y$ 
10: return  $performance$ 

```

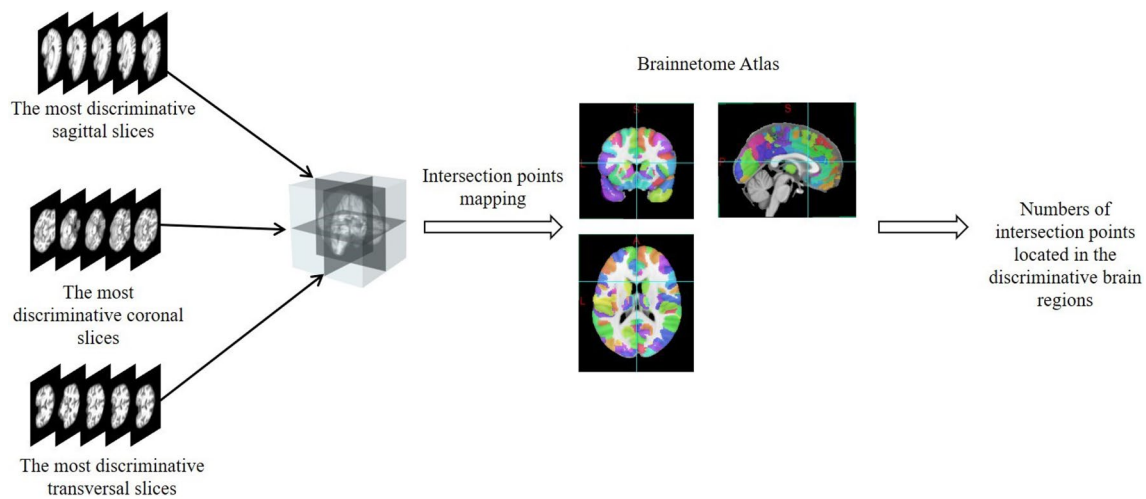


**Fig. 4** The discriminative brain regions ranked by the number of the points of intersection located in them

Here, *chrom* represents a chromosome, *L* is the length of the chromosome, and *pos* is the position (i.e., sequence number) of the gene to be flipped in the chromosome. *chrom(pos)* is the value of the gene on the position *pos* in the chromosome (i.e., the gene *pos*), and the value “1” or “0” indicates the base classifier corresponding to the gene *pos* is or is NOT selected, respectively. *mp(pos)* is the mutation probability of the gene *pos*. *p* is the initial rate of the GA mutation probability, the mutation probability used in the GA optimization process is *mp*, instead of the initial mutation rate *p*.

Algorithm 2 was utilized for calculating the fitness value of a chromosome. In detail, the classification results from the selected base classifiers, i.e., those corresponding to the genes with value of 1 in a chromosome, were finally integrated to obtain the classification result of the chromosome, which was used as the fitness value of the chromosome. The optimization goal was to maximize the fitness value of a chromosome. With the operations of selection, crossover and mutation, etc., an optimal chromosome individual might be obtained. Accordingly, we could adaptively obtain the optimal combination of base classifiers and the final classification results on testing dataset might be achieved.

### 2.2.5 Genome-Wide Association Studies

Here, the purpose of GWAS is to identify SNPs statistically significantly contributing to differences in gray matter volumes of the identified discriminative brain regions for AD. Aiming to estimate if or not the correlation of a SNP with the gray matter volumes of a specific brain region is statistically significant, two hypotheses against each other, i.e., *H0* and *H1*, need to be tested on our collected data. In the *H0*

**Table 3** Comparison of experimental results

Experiment	Method	ACC	AUC	MCC
AD vs.HC	PCA + SVM [26]	0.76 ± 0.11	–	–
	CNN-EL	0.80 ± 0.05	0.90 ± 0.03	0.61 ± 0.10
	CNN-EL-GA	0.86 ± 0.05	0.92 ± 0.04	0.72 ± 0.10
MCIc vs.HC	PCA + SVM [26]	0.72 ± 0.12	–	–
	CNN-EL	0.79 ± 0.04	0.80 ± 0.06	0.49 ± 0.11
	CNN-EL-GA	0.80 ± 0.03	0.82 ± 0.04	0.53 ± 0.09
MCIc vs.MCIc	PCA + SVM [26]	0.66 ± 0.16	–	–
	CNN-EL	0.64 ± 0.04	0.65 ± 0.07	0.11 ± 0.12
	CNN-EL-GA	0.66 ± 0.04	0.61 ± 0.06	0.21 ± 0.04

hypothesis, a model indicating that the SNP does not have impact on the phenotype [31] is assumed.

The *H0* hypothesis assumes only the population mean  $\mu$  and the environment *e* affect the phenotype *y*. If the collected data do not exhibit otherwise, the *H0* hypothesis is suggested to be true.

As shown in formula 3, a model specifying that the SNP is significantly correlated with the phenotype is assumed in the *H1* hypothesis.

$$y = \mu \mathbf{1} + \beta_k X_k + e \tag{3}$$

Here, the column vector *y* represents the gray matter volumes of a specific brain region of all of the subjects in the dataset;  $X_k$  and *e* are a column containing the genotypes for the *k*–*th* variant in all the subjects and a random vector containing the environments, respectively.  $\mathbf{1}$  is a column vector of 1 s.  $\beta_k$  denotes the effect of the *k*–*th* variant on the gray matter volumes of a specific brain region, and  $\mu$  is the model mean.

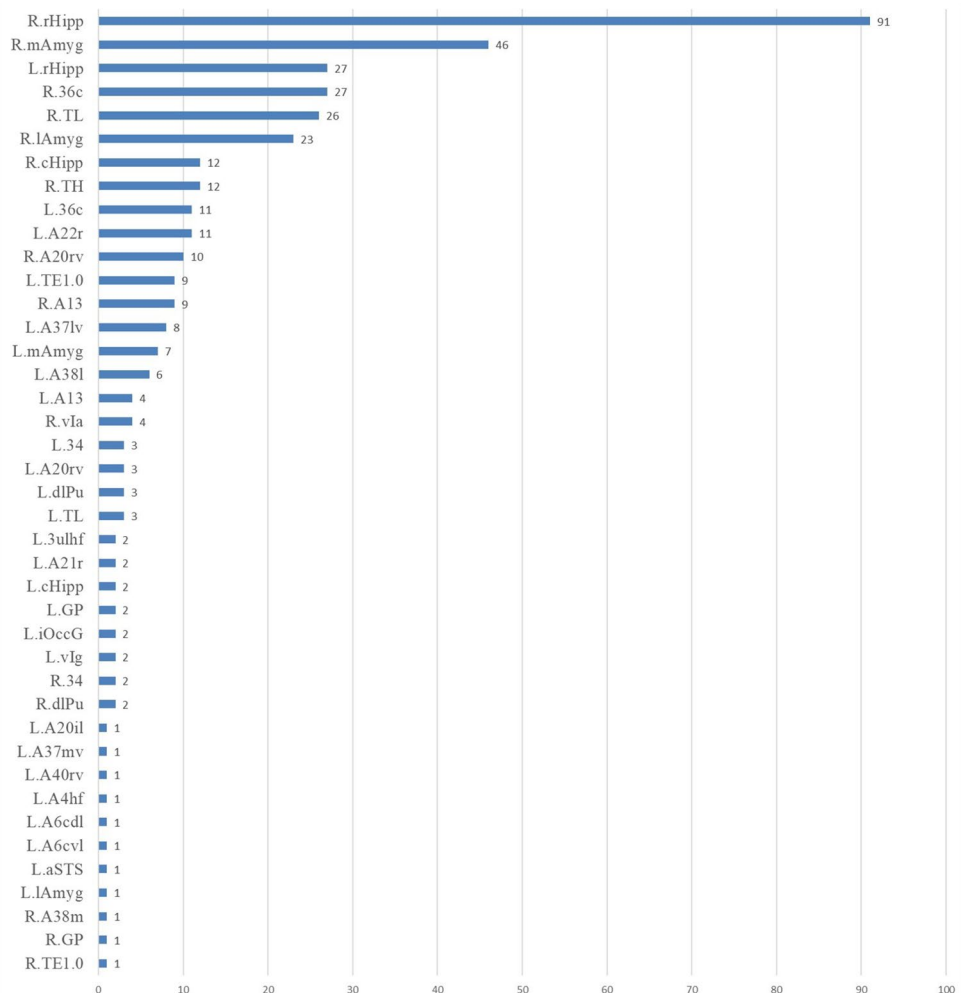
In the *H1* hypothesis, besides the population mean  $\mu$  and environment  $e$ , the genotype  $x$  has an influence on the phenotypes  $y$  as well. That is, presence of the SNP indicates a subject is prone to having the trait. In formula 3,  $\beta$  is utilized to quantitatively measure the impact of the SNP on the gray matter volumes of a specific brain region. If the collected data fit formula 3 beyond a specific threshold, the SNP is assumed to be significantly correlated with the gray matter volumes of a specific brain region.

In GWAS, when the involved phenotype is a qualitative trait, the logistic regression model is usually utilized. Meanwhile, when the phenotype is a quantitative trait, the ordinary linear regression model is often employed. Here, the involved phenotype was the gray matter volumes of the identified discriminative brain regions, which is a quantitative trait. Thus, the ordinary linear regression model was used in this study.

In each of the three binary classification tasks, the slices corresponding to the trained base classifiers in the optimal combination were supposed as those with the strongest discriminability for AD identification. Therefore, we

determined the points of intersection with the above-mentioned discriminative slices involved in the optimal combination. And then, these points were mapped into the standard MNI (Montreal Neurological Institute) space. In this way, the number of the points of intersection acted as an indicator to measure the AD discriminability for a brain region where the points were located. Here, with the help of the Brainnetome Atlas, the brain regions with more points of intersection were considered as those more contributing to AD identification. Next, the top ten brain regions with the ten most points of intersection were selected and their gray matter volumes were calculated with FreeSurfer. The procedure for calculating the numbers of the points of intersection is exhibited in Fig. 4. The obtained gray matter volumes were acted as phenotypic data of subsequent GWAS experiments.

**Fig. 5** Numbers of points of intersection located in the discriminative brain regions





## 3 Experiment Results

### 3.1 Classification Results

A total of 736 3D MRI images of 736 subjects from the ADNI database were divided into the training and testing datasets ( $n=458$ ; Table 1), which were utilized to train base classifiers and evaluate the effectiveness of the final classifier ensemble based on three-axis slices, and a validation dataset ( $n=278$ ; Table 2) which was employed to examine and optimize the combination of base classifiers. The stratified fivefold cross-validation procedure was strictly followed in the training and testing stages for each binary classification task, i.e., AD vs. HC, MCIc vs. HC and MCIc vs. MCInc. Any image in the training/testing dataset was NOT utilized to optimize the combination of trained base classifiers so as to avoid potential data leakage in all of binary classification tasks.

The number of epoch was set as 30 for training each CNN base classifier. All convolutional layer activation functions of all the base classifiers were LReLU [32], and Adam [33] was used for gradient update algorithm. The batch size and the learning rate were set to 200 and 0.0001, respectively. The chromosome population size of genetic algorithm, i.e.,  $m$ , was 30, and the initial values of crossover probability  $C_p$  and mutation probability  $p$  were set to 0.75 and 0.05, respectively. The maximum number of iterations was set as 10,000.

The experimental results obtained with the proposed CNN-EL-GA approach were compared with those achieved with the method based on PCA and SVM, i.e., PCA + SVM [26], which was shown in Table 3. The classification accuracy of each binary classification task, i.e., AD vs. NC, MCIc vs. NC and MCIc vs. MCInc, on the testing dataset was 86%, 80% and 66%, respectively. It showed that average classification accuracies for AD vs. HC and MCIc vs. HC achieved with the proposed CNN-EL-GA were obviously higher than those obtained with the method based on PCA + SVM, while the average classification accuracy for MCIc vs. MCInc was not obviously higher though the standard deviation was substantially lower. As for the reason why the classification accuracy for MCIc vs. MCInc task was relatively low, we supposed that the proposed method in a data-driven way usually demanded more training data and was negatively affected by the insufficient training samples to a great extent in the MCIc vs. MCInc task. To clearly exhibit the effectiveness of GA in promoting the classification results, the advocated CNN-EL-GA with its non-GA-based version, i.e., CNN-EL [34]. The comparison results given in Table 3 showed that GA played an important role in significantly improving the performance of the classification.

### 3.2 Phenotypic Data

To conduct GWAS experiments, the phenotypic data need to be prepared in advance. Here, each an MRI slice was independently employed to build a single-slice base classifier. In this way, while the most discriminative single-slice base classifiers were selected on the validation dataset with GA in each of three binary classification tasks, the corresponding sagittal, coronal, and transverse slices were determined at the same time and supposed to be the most AD discriminative among all the slices. Thus, the points of intersections of the determined coronal, sagittal, and transverse slices were mapped onto the brain regions using Brainnetome Atlas. Because the resulting points of intersection were located on the most AD discriminative coronal, sagittal, and transverse slices simultaneously, we cannot deny that the number of the points of intersection located in a brain region was capable of acting as an indicator to evaluate the AD discriminability for the brain region. The brain regions with the most points of intersection were considered as the most discriminative among all the brain regions. In addition, it is notable that some points of intersection appeared in the unlabeled brain regions in the Brainnetome Atlas.

We ranked the brain regions in descending order on the basis of the number of points of intersection located in them, as exhibited in Fig. 5. In the figure, values on the horizontal axis denote the total number of points of intersection in each a discriminative brain region, which were obtained with stratified five-fold cross-validation procedure for all of three binary classification tasks. That is, for each a brain region, all the intersection points in the brain region obtained with stratified five-fold cross-validation method in all the three binary classification tasks were summed up in each of brain regions. And then, the brain regions could be ranked by the number of the intersection points located in them. Those values on the vertical axis denote the brain region labels. The two prefix capital letters, i.e., “L” or “R” of a brain region label (e.g., L.rHipp and R.mAmyg) represent the left or the right cerebral hemisphere, respectively.

Thus, the top ten most discriminative brain regions (i.e., R.rHipp, R.mAmyg, L.rHipp, R.36c, R.TL, R.lAmyg, R.cHipp, R.TH, L.36c, L.A22r) shown in Fig. 5 were considered as those most significantly correlated with AD detection. The gray matter volume values of the ten brain regions from 458 subjects were acquired with FreeSurfer and served as the phenotypic data in the following GWAS analysis.

### 3.3 GWAS Results

We conducted ten GWAS on ten brain morphological traits, i.e., gray matter volumes of the top ten brain regions, respectively. In the experiments, the statistical significance (i.e.,  $p$  value) of the associations between each SNP and each of ten

traits was assessed by an ordinary linear regression model using PLINK. And then, according to the obtained p-values, Manhattan plots were drawn (See Figs. 1, 2, 3, 4, 5, 6, 7, 8, 9, 10 in Appendix) to visually display the SNPs with the most significant correlation with the traits. In the figures, values on the vertical axis represent the negative logarithm of p values. A genome-wide significance p value threshold was set a priori at  $1 \times 10^{-5}$ . Chromosome 23, 24, 25 and 26 actually indicate the X chromosome, the Y chromosome, the pseudo-autosomal region of X, Y chromosomes, and the mitochondrial region, respectively. Plus, for the sake of simplicity, the points with the negative logarithms of p values which are higher than 8 are located on the line with the negative logarithms of p values which are the same as 8.

After querying the SNPs identified as most highly correlated with the gray matter volumes of the ten brain regions in the ten GWAS experiments through the website <https://www.ncbi.nlm.nih.gov/snp>, we have obtained detailed information on those SNPs (See Table 1 in Appendix). Seven SNPs (i.e., rs36088804, rs2578907, rs2556924, rs2563370, rs34045151, rs2578811 and rs2522623) located in the gene Protocadherin 11 X-linked (PCDH11X) were found to statistically significantly occur 26 times in total in the ten GWAS experiments. Meanwhile, we found that the SNP (rs34640393) located in the gene protocadherin 11 Y-linked (PCDH11Y), a gene unique to Homo males that encodes Protocadherin 11Y, statistically significantly appeared in four of ten GWAS experiments. In [35], genetic variation in PCDH11X was suggested to be associated with late-onset AD (LOAD), the only GWAS signal on the X chromosome currently. However, [36] indicated independent replication of this finding had not been consistent. In fact, [37] pointed out that the PCDH11X/Y genes were a cell surface receptor molecule belonging to the protocadherin gene, a subfamily of the cadherin superfamily. Similar to other cadherins, it was cleaved by  $\gamma$ -secretase and mediated cell–cell adhesion. Cadherins formed the complex together with PS1/ $\gamma$ -secretase and regulated cell–cell interaction after the cleavage by  $\gamma$ -secretase. Familial AD mutations in PS1 inhibited this process. Thus, PCDH11X/Y were considered to take part in cell signaling which was very important in the growth of the central nervous system [35].

Kantojarvi [38] advocated that PCDH11X/Y were located in a human XY homology region on Xq21.31 in loci where two SNPs (rs5941380 and rs35429716) were exhibited to be significant correlation with autism. Plus, it's found that the SNP (rs2451078) located in the gene TPTE2 was strongly statistically significant, which occurred in five of ten GWAS experiments. That indicated that the SNP was closely related to the gray matter volumes of these brain regions and might be a candidate AD genetic biomarker. [39] revealed that the SNP (rs2451078), discovered in the CIDR/Pankratz et al. 2009 dataset [40], had reached genome-wide significance

( $p$  value  $< 1.94 \times 10^{-10}$ ), though it was not reproduced in another dataset, e.g., the Ashkenazi Jewish [39]. Furthermore, it was found that the SNP (rs2451078) allegedly located on autosomes exhibited significant difference in genotype frequencies between men and women [41]. Plus, rs17016520 and rs10496214, which are located in the gene LOC107985902, exhibited statistical significance twice in the ten GWAS experiments, respectively. That means they could be worthwhile for further investigation. Moreover, in [42], rs10496214 was found to be one of schizophrenia SNPs significantly associated and concordant in both the Munich and Aberdeen Collections. It seemed that the SNP rs17016520 has not been yet further studied so far. Moreover, nine variants (i.e., rs2591590, rs2591591, rs2591593, rs1862462, rs2591597, rs1867691, rs2547072, rs2591594 and rs2547076) located in the MUC16 gene were discovered to be statistically significantly associated with the gray matter volumes of the ten brain regions. Staley [43] indicated that MUC16 was shown to form a protective mucous barrier on the apical surfaces of the epithelia and it was associated with the following disorders: ovarian cancer, endometriosis, pseudo-meigs syndrome, serous cystadenocarcinoma and bronchogenic cyst. In addition, we found that three variants, i.e., rs4543320, rs9352767 and rs6903123, located in the LINC01621 gene was of statistical significance in ten GWAS experiments. To sum up, six genes of PCDH11X/Y, TPTE2, LOC107985902, MUC16 and LINC01621 and the variants, such as rs36088804, rs34640393, rs2451078, rs10496214, rs17016520, rs2591597, rs9352767 and rs5941380 etc., were discovered as the potential genetic biomarkers for AD, which would be interesting for follow-up studies.

## 4 Discussion

In this study, we advocated an adaptive classifier ensemble model combining CNN and EL with GA to distinguish AD or MCIC from HC, and MCIC from MCInc. Meanwhile, the ten most discriminative brain regions were identified and their gray matter volumes were obtained. Based on these, GWAS experiments were conducted to explore the candidate genetic biomarkers for AD.

With the proposed model, we obtained average classification performance (i.e., accuracy  $\pm$  standard deviation) of  $0.86 \pm 0.05$ ,  $0.80 \pm 0.03$ , and  $0.66 \pm 0.04$  for AD vs. HC, MCIC vs. HC, and MCIC vs. MCInc, respectively. Compared with a PCA + SVM method [26], the advocated method could automatically learn the discriminative representations from the MRI images to further enhance the robustness and generalization of the acquired model. Meanwhile, in comparison with the CNN-EL method [22], the proposed method introduced GA as the optimization strategy to adaptively select the base classifiers globally in a data-driven

way, which was more objective and less dependent on prior knowledge and hyper-parameters. The comparison results showed that accuracies achieved with the CNN-EL-GA were better than those obtained with the CNN-EL method [22] for all the three binary classification tasks.

Furthermore, when experimental results (e.g., the identified discriminative brain regions, SNPs and genes) in this study were compared with those in [34], it is notable that the results in the this study and [34] were similar to some extent though the datasets and the approach utilized in [34] were different from those in this study and any SNPs in the X and Y chromosomes, the pseudo-autosomal region (XY), and mitochondrial region (that is, only SNPs in Chromosomes 1–22 were analyzed) were excluded for all analyses in [34]. In detail, the subjects involved in the datasets utilized to locate the discriminative brain regions were NOT the same as those involved in the datasets subsequently employed to conduct the GWAS experiments in [34]. Also, the CNN-EL approach, rather than the CNN-EL-GA, was employed to discern the most discriminative brain regions to classify AD in [34].

Actually, in comparison of those in [34], the observed similarity in the experimental results in this study exhibited the robustness and effectiveness of the CNN-EL-GA approach proposed here to some degree. After all, the datasets utilized in this study and [34] were NOT the same since the subjects involved in the datasets utilized to identify the discriminative brain regions were forced to be the same as those involved in the datasets subsequently employed to conduct the GWAS experiments in this study. And the experimental results have indicated that the generalization ability of the classifier ensemble achieved with CNN-EL-GA proposed here was substantially better than that of the ensemble obtained with CNN-EL.

As a matter of fact, in [44] and [45], new technical frameworks have been proposed to identify AD patients and discover some brain regions and genes associated with AD significantly. The focus in these two papers is multimodal data fusion. However, in this paper, the goal is to discover the genetic biomarkers based on the framework of Genome-Wide Association Studies (GWAS), which has been widely accepted to identify disease genes by examining the relationship between each SNP and phenotype traits. As for phenotype traits in GWAS, generally speaking, it is better to select the quantitative phenotype, which is related to the disease and is easy and accurate to measure. To obtain more suitable quantitative phenotype traits, we proposed the CNN-EL-GA method to determine the most discriminative brain regions in a data-driven manner while the obtained ensemble model exhibited the best generalization performance on the testing dataset. And then, the gray matter volumes of these determined brain regions acted as the quantitative phenotype

traits in the GWAS experiments to help identify candidate neuroimaging biomarkers for brain diseases.

All in all, the major contributions of this study were as follows.

1. To reduce the negative impact of subjective factors and to restrict the dependence on prior knowledge, GA was utilized to adaptively select the optimal combination of the base classifiers trained using coronal, sagittal or transverse slices in a data-driven way to build the ensemble model in the presented CNN-EL-GA approach and resulting, a better classification performance was further achieved.
2. With the help of the advanced CNN-EL-GA approach, the most discriminative coronal, sagittal and transverse slices in all three binary classification tasks, respectively, determined the points of intersection. And then, using the Brainnetome Atlas, these points were mapped to the brain regions. For a brain region, the sum of all the numbers of the points of intersection located in the brain region obtained with the five-fold cross-validation method in the three binary classification tasks were calculated to measure its capability of aiding the diagnosis of AD. Gray matter volumes of the selected brain regions were calculated and sorted to facilitate identifying the SNPs and genes correlated to the traits as candidate genetic biomarkers for AD with GWAS. According to the analysis of ten GWAS experimental results, six genes, i.e., PCDH11X/Y, TPTE2, LOC107985902, MUC16 and LINC01621, and the variants, e.g., rs36088804, rs34640393, rs2451078, rs10496214, rs17016520, rs2591597, rs9352767 and rs5941380, were obtained. In addition, studies have shown that the PCDH11X/Y genes were AD susceptibility genes [35] and strong associated with autism [38] and that the SNPs, i.e., rs2451078 and rs10496214, had significant relationships with Parkinson's disease [39] and schizophrenia [42], respectively.
3. The method proposed in this study might also be useful for identifying candidate neuroimaging and genetic biomarkers for other brain disorders, e.g., autism, Parkinson's disease, severe depression and schizophrenia, especially for other little-investigated brain diseases, in a data-driven manner. The methods could effectively help focus on those biomarkers that are most likely to be informative, and might be expected to facilitate the research progress of the brain disorders. In the future research, the generalizability of the proposed method on other brain disorders and the clinical implications of the obtained findings will be further investigated.

In this study, gray matter volume values of the most discriminative brain regions acted as the phenotype data in the

GWAS experiments. A natural question is whether or not there is any morphological parameter which is more suitable to be the phenotypic data in the GWAS experiments than the gray matter volume value. It might be worthy of being investigated in the future research.

## 5 Conclusion

In conclusion, to help discover more effective AD biomarkers in a data-driven manner, we advanced an adaptive classifier ensemble model, i.e., CNN-EL-GA, to distinguish the subjects with MCI or AD in the three binary classification tasks using sMRI. In each binary classification task, a lot of base classifiers were built utilizing coronal, sagittal, or transverse MRI slices, and those with strong discriminability were then selected and ensembled with GA. The results showed an accuracy rate of 0.86 for AD vs. HC, 0.80 for MCIc vs. HC, and 0.66 for MCIc vs. MCInc. When the generalization capability of the acquired classifier ensemble was maximized, the slices corresponding to the selected built base classifiers in the acquired classifier ensemble were thought to be those with the strongest capabilities to identify AD. Thus, the points of intersection were determined with the most discriminative coronal, sagittal, and transverse slices. The gray matter volumes of the top ten discriminative brain regions, which contained the most intersection points, were employed to conduct GWAS together with the genotype data. In the experimental results, six genes of PCDH11X/Y, TPTE2, LOC107985902, MUC16 and LINC01621 and the SNPs including rs36088804, rs34640393, rs2451078, rs10496214, rs17016520, rs2591597, rs9352767 and rs5941380 were identified. They could act as candidate genetic biomarkers for AD. Through comparing the results with the previously reported findings, we could see that this approach might overcome the limitations associated with subjective factors and the dependence on prior knowledge while adaptively achieving more robust and effective candidate biomarkers in a data-driven manner. The approach is promising to improve the discovery of effective genetic biomarkers for brain disorders, as well as to help improve the effectiveness of identified candidate neuroimaging biomarkers for brain diseases.

**Supplementary Information** The online version contains supplementary material available at <https://doi.org/10.1007/s12539-021-00470-3>.

**Acknowledgements** We thank the reviewers for their constructive comments on this article. This study was supported by NSF of China (Grant Nos. 61976058, 61772143 and U19A2067), National Key RD Program of China (Grant No. 2018YFC0910405), Science and Technology Planning Project of Guangdong (Grant No. 2021A1515012300, 2019A050510041 and 2020A1515010941), and Science and Technology Planning Project of Guangzhou (Grant Nos. 202103000034 and 202002020090). Additional funding for neurological research was from

Surrey Hospital & Outpatient Centre Foundation (FHG2017-001). Data collection and sharing for this project were funded by the Alzheimer's Disease Neuroimaging Initiative (ADNI) (National Institutes of Health Grant U01 AG024904) and DOD ADNI (Department of Defense Award No. W81XWH-12-2-0012). ADNI was funded by the National Institute on Aging, the National Institute of Biomedical Imaging and Bioengineering, and through generous contributions from the following: AbbVie, Alzheimer's Association; Alzheimer's Drug Discovery Foundation; Araclon Biotech; BioClinica, Inc.; Biogen; Bristol-Myers Squibb Company; CereSpir, Inc.; Cogstate; Eisai Inc.; Elan Pharmaceuticals, Inc.; Eli Lilly and Company; EuroImmun; F. Hoffmann-La Roche Ltd and its affiliated company Genentech, Inc.; Fujirebio; GE Healthcare; IXICO Ltd.; Janssen Alzheimer Immunotherapy Research & Development, LLC.; Johnson & Johnson Pharmaceutical Research & Development LLC.; Lumosity; Lundbeck; Merck & Co., Inc.; Meso Scale Diagnostics, LLC.; NeuroRx Research; Neurotrack Technologies; Novartis Pharmaceuticals Corporation; Pfizer Inc.; Piramal Imaging; Servier; Takeda Pharmaceutical Company; and Transition Therapeutics. The Canadian Institutes of Health Research was providing funds to support ADNI clinical sites in Canada. Private sector contributions are facilitated by the Foundation for the National Institutes of Health ([www.fnih.org](http://www.fnih.org)). The grantee organization is the Northern California Institute for Research and Education, and the study is coordinated by the Alzheimer's Therapeutic Research Institute at the University of Southern California. ADNI data are disseminated by the Laboratory for Neuro Imaging at the University of Southern California. Additional funding support for the manuscript preparation was from the Surrey Hospital & Outpatient Centre Foundation of Fraser Health, Canada.

## Declarations

**Conflict of interest** The authors declare that they have no conflict of interest.


## References

- Hong-meng L, Di Z, Xue-bin C (2017) Deep learning for early diagnosis of Alzheimer's disease based on intensive alexnet. *Comput Sci* 44(6):50–59. <https://doi.org/10.11896/j.issn.1002-137X.2017.6A.011>
- Prince M, Wimo A, Guerchet M, Ali G, Wu Y, Prina M (2015) World Alzheimer report 2015. the global impact of dementia. Alzheimer's Disease International (ADI), London
- Liu S, Liu S, Cai W, Pujol S, Kikinis R, Feng D (2014) Early diagnosis of Alzheimer's disease with deep learning. *Int Sympos Biomed Imaging*. <https://doi.org/10.1109/ISBI.2014.6868045>
- Frisoni GB, Fox NC, Jack CR, Scheltens P, Thompson PM (2010) The clinical use of structural MRI in Alzheimer disease. *Nat Rev Neurol* 6(2):67–77. <https://doi.org/10.1038/nrneurol.2009.215>
- Hao X, Bao Y, Guo Y, Yu M, Zhang D, Risacher SL, Saykin AJ, Yao X, Shen L, Initiative ADN et al (2020) Multi-modal neuroimaging feature selection with consistent metric constraint for diagnosis of Alzheimer's disease. *Med Image Anal* 60:101625. <https://doi.org/10.1016/j.media.2019.101625>
- Jie B, Liu M, Liu J, Zhang D, Shen D (2016) Temporally constrained group sparse learning for longitudinal data analysis in Alzheimer's disease. *IEEE Trans Biomed Eng* 64(1):238–249. <https://doi.org/10.1109/tbme.2016.2553663>
- Liu M, Li F, Yan H, Wang K, Ma Y, Shen L, Xu M, Initiative ADN et al (2020) A multi-model deep convolutional neural network for automatic hippocampus segmentation and classification in Alzheimer's disease. *Neuroimage* 208:116459. <https://doi.org/10.1016/j.neuroimage.2019.116459>

8. Liu M, Zhang D, Adeli E, Shen D (2015) Inherent structure-based multiview learning with multitemplate feature representation for Alzheimer's disease diagnosis. *IEEE Trans Biomed Eng* 63(7):1473–1482. <https://doi.org/10.1109/tbme.2015.2496233>
9. Liu M, Zhang J, Adeli E, Shen D (2018) Joint classification and regression via deep multi-task multi-channel learning for Alzheimer's disease diagnosis. *IEEE Trans Biomed Eng* 66(5):1195–1206. <https://doi.org/10.1109/tbme.2018.2869989>
10. Tong T, Gao Q, Guerrero R, Ledig C, Chen L, Rueckert D, Initiative ADN et al (2016) A novel grading biomarker for the prediction of conversion from mild cognitive impairment to Alzheimer's disease. *IEEE Trans Biomed Eng* 64(1):155–165. <https://doi.org/10.1109/TBME.2016.2549363>
11. Zeng N, Qiu H, Wang Z, Liu W, Zhang H, Li Y (2018) A new switching-delayed-PSO-based optimized SVM algorithm for diagnosis of Alzheimer's disease. *Neurocomputing* 320:195–202. <https://doi.org/10.1016/j.neucom.2018.09.001>
12. Zhou T, Thung KH, Liu M, Shen D (2018) Brain-wide genome-wide association study for Alzheimer's disease via joint projection learning and sparse regression model. *IEEE Trans Biomed Eng* 66(1):165–175. <https://doi.org/10.1109/tbme.2018.2824725>
13. Rathore S, Habes M, Iftikhar MA, Shacklett A, Davatzikos C (2017) A review on neuroimaging-based classification studies and associated feature extraction methods for Alzheimer's disease and its prodromal stages. *Neuroimage* 155:530–548. <https://doi.org/10.1016/j.neuroimage.2017.03.057>
14. LeCun Y, Bottou L, Bengio Y, Haffner P (1998) Gradient-based learning applied to document recognition. *Proc IEEE* 86(11):2278–2324. <https://doi.org/10.1109/5.726791>
15. Litjens G, Kooi T, Bejnordi BE, Setio AAA, Ciompi F, Ghafoorian M, Van Der Laak JA, Van Ginneken B, Sanchez CI (2017) A survey on deep learning in medical image analysis. *Med Image Anal* 42:60–88. <https://doi.org/10.1016/j.media.2017.07.005>
16. Shen D, Wu G, Suk HI (2017) Deep learning in medical image analysis. *Annu Rev Biomed Eng* 19:221–248. <https://doi.org/10.1146/annurev-bioeng-071516-044442>
17. Hosseini-Asl E, Keynton R, El-Baz A (2016) Alzheimer's disease diagnostics by adaptation of 3d convolutional network. *IEEE Int Conf Image Process*. <https://doi.org/10.1109/ICIP.2016.7532332>
18. Jain R, Jain N, Aggarwal A, Hemanth DJ (2019) Convolutional neural network based Alzheimer's disease classification from magnetic resonance brain images. *Cogn Syst Res* 57:147–159. <https://doi.org/10.1016/j.cogsys.2018.12.015>
19. Kruthika K, Maheshappa H, Initiative ADN et al (2019) Cbir system using capsule networks and 3d cnn for Alzheimer's disease diagnosis. *Inform Med Unlocked* 14:59–68. <https://doi.org/10.1016/j.imu.2019.100227>
20. Tanveer M, Richhariya B, Khan R, Rashid A, Khanna P, Prasad M, Lin C (2020) Machine learning techniques for the diagnosis of Alzheimer's disease: A review. *ACM Trans Multimed Comput Commun Appl* 16(1):1–35. <https://doi.org/10.1145/3344998>
21. Wang H, Shen Y, Wang S, Xiao T, Deng L, Wang X, Zhao X (2019) Ensemble of 3d densely connected convolutional network for diagnosis of mild cognitive impairment and Alzheimer's disease. *Neurocomputing* 333:145–156. <https://doi.org/10.1016/j.neucom.2018.12.018>
22. Pan D, Zeng A, Jia L, Huang Y, Frizzell T, Song X (2020) Early detection of Alzheimer's disease using magnetic resonance imaging: a novel approach combining convolutional neural networks and ensemble learning. *Front Neurosci*. <https://doi.org/10.3389/fnins.2020.00259>
23. Hariri AR, Weinberger DR (2003) Imaging genomics. *Br Med Bull* 65(1):259–270. <https://doi.org/10.1002/9783527678679.dg05936>
24. Chauhan G, Adams HH, Bis JC, Weinstein G, Yu L, Toghlofer AM, Smith AV, Van Der Lee SJ, Gottesman RF, Thomson R et al (2015) Association of Alzheimer's disease gwas loci with mri markers of brain aging. *Neurobiol Aging* 36(4):1765–e7. <https://doi.org/10.1016/j.neurobiolaging.2014.12.028>
25. Tan L, Yu JT, Zhang W, Wu ZC, Zhang Q, Liu QY, Wang W, Wang HF, Ma XY, Cui WZ (2013) Association of GWAS-linked loci with late-onset Alzheimer's disease in a northern Han Chinese population. *Alzheimer's Dement* 9(5):546–553. <https://doi.org/10.1016/j.jalz.2012.08.007>
26. Salvatore C, Cerasa A, Battista P, Gilardi MC, Quattrone A, Castiglioni I (2015) Magnetic resonance imaging biomarkers for the early diagnosis of Alzheimer's disease: a machine learning approach. *Front Neurosci* 9:307. <https://doi.org/10.3389/fnins.2015.00307>
27. Chang CC, Chow CC, Tellier LC, Vattikuti S, Purcell SM, Lee JJ (2015) Second-generation PLINK: rising to the challenge of larger and richer datasets. *GigaScience*. <https://doi.org/10.1186/s13742-015-0047-8>
28. Fischl B (2012) FreeSurfer. *Neuroimage* 62(2):774–781. <https://doi.org/10.1016/j.neuroimage.2012.01.021>
29. Fan L, Li H, Zhuo J, Zhang Y, Wang J, Chen L, Yang Z, Chu C, Xie S, Laird AR, Fox PT, Eickhoff SB, Yu C, Jiang T (2016) The human brainnetome atlas: a new brain atlas based on connectonal architecture. *Cereb Cortex* 26(8):3508–3526. <https://doi.org/10.1093/cercor/bhw157>
30. Wang SH, Phillips P, Sui Y, Liu B, Yang M, Cheng H (2018) Classification of Alzheimer's disease based on eight-layer convolutional neural network with leaky rectified linear unit and max pooling. *J Med Syst*. <https://doi.org/10.1007/s10916-018-0932-7>
31. Sul JH, Martin LS, Eskin E (2018) Population structure in genetic studies: Confounding factors and mixed models. *PLoS Genet* 14(12):e1007309. <https://doi.org/10.1371/journal.pgen.1007309>
32. Liew SS, Khalil-Hani M, Bakhteri R (2016) Bounded activation functions for enhanced training stability of deep neural networks on visual pattern recognition problems. *Neurocomputing* 216:718–734. <https://doi.org/10.1016/j.neucom.2016.08.037>
33. Kingma DP, Ba J (2015) Adam: A method for stochastic optimization. In: Bengio Y, LeCun Y (eds) International Conference on Learning Representations, Conference Track Proceedings, ICLR 2015, San Diego, CA, USA, May 7–9, 2015
34. Pan D, Huang Y, Zeng A, Jia L, Song X, A.D.N.I. et al (2019) Early diagnosis of Alzheimer's disease based on deep learning and GWAS. International workshop on human brain and artificial intelligence. Springer, Berlin, pp 52–68. [https://doi.org/10.1007/978-981-15-1398-5\\_4](https://doi.org/10.1007/978-981-15-1398-5_4)
35. Carrasquillo MM, Zou F, Pankratz VS, Wilcox SL, Ma L, Walker LP, Younkin SG, Younkin CS, Younkin LH, Bisceglia GD et al (2009) Genetic variation in PCDH11X is associated with susceptibility to late-onset Alzheimer's disease. *Nat Genet* 41(2):192–198. <https://doi.org/10.1038/ng.305>
36. Beecham GW, Naj A, Gilbert JR, Haines JL, Buxbaum JD, Pericak-Vance MA (2010) PCDH11X variation is not associated with late-onset Alzheimer disease susceptibility. *Psychiatr Genet* 20(6):321. <https://doi.org/10.1097/YPG.0b013e32833b635d>
37. Rosenberg RN, Lambracht-Washington D, Yu G, Xia W (2016) Genomics of Alzheimer disease: a review. *JAMA Neurol* 73(7):867–874. <https://doi.org/10.1001/jamaneurol.2016.0301>
38. Kantojarvi K (2013) Exploring genetic susceptibility to autism spectrum disorders. Academic Dissertation, University of Helsinki
39. Liu X, Cheng R, Verbitsky M, Kisselev S, Browne A, Mejia-Sanatana H, Louis ED, Cote LJ, Andrews H, Waters C et al (2011) Genome-wide association study identifies candidate genes for

- Parkinson's disease in an Ashkenazi Jewish population. *BMC Med Genet* 12(1):104. <https://doi.org/10.1186/1471-2350-12-104>
40. Pankratz N, Wilk JB, Latourelle JC, DeStefano AL, Halter C, Pugh EW, Doheny KF, Gusella JF, Nichols WC, Foroud T, Richard HM (2008) Genomewide association study for susceptibility genes contributing to familial Parkinson disease. *Hum Genet* 124(6):593–605. <https://doi.org/10.1007/s00439-008-0582-9>
  41. Galichon P, Mesnard L, Hertig A, Stengel B, Rondeau E (2012) Unrecognized sequence homologies may confound genome-wide association studies. *Nucleic Acids Res* 40(11):4774–4782. <https://doi.org/10.1093/nar/gks169>
  42. Jean PS (2008) Genes associated with schizophrenia identified using a whole genome scan. US Patent App. 11/970,611
  43. Staley LA (2018) Analysis of whole exome sequence data in affected cousin pairs from high-risk Alzheimer's pedigrees. In: Master thesis, all Theses and Dissertations, Brigham Young University, p 7332
  44. Bi XA, Liu Y, Xie Y, Hu X, Jiang Q (2020) Morbigenous brain region and gene detection with a genetically evolved random neural network cluster approach in late mild cognitive impairment. *Bioinformatics* 36(8):2561–2568. <https://doi.org/10.1093/bioinformatics/btz967>
  45. Bi XA, Hu X, Wu H, Wang Y (2020) Multimodal data analysis of Alzheimer's disease based on clustering evolutionary random forest. *IEEE J Biomed Health Inform* 24(10):2973–2983. <https://doi.org/10.1109/jbhi.2020.2973324>

## Authors and Affiliations

An Zeng<sup>1</sup> · Huabin Rong<sup>1</sup> · Dan Pan<sup>2</sup>  · Longfei Jia<sup>1</sup> · Yiqun Zhang<sup>1</sup> · Fengyi Zhao<sup>1</sup> · Shaoliang Peng<sup>3</sup> · for the Alzheimer's Disease Neuroimaging Initiative (ADNI)

<sup>1</sup> Faculty of Computer, Guangdong University of Technology, Guangzhou 510006, People's Republic of China

<sup>2</sup> School of Electronics and Information, Guangdong Polytechnic Normal University, Guangzhou 510665, People's Republic of China

<sup>3</sup> College of Computer Science and Electronic Engineering, Hunan University, School of Computer Science, National University of Defense Technology, Peng Cheng Lab, Shenzhen 518000, People's Republic of China